SCIENTIFIC REPORTS

OPEN

The electronic properties of impurities (N, C, F, Cl, and S) in Ag_3PO_4: A hybrid functional method study

Received: 09 March 2015
Accepted: 09 July 2015
Published: 03 August 2015

Yang Huang[1], Tai Ma[1], Qing-yuan Chen[1], Chao Cao[2] & Yao He[1]

The transition energies and formation energies of N, C, F, Cl, and S as substitutional dopants in Ag_3PO_4 are studied using first-principles calculations based on the hybrid Hartree-Fock density functional, which correctly reproduces the band gap and thus provides the accurate defect states. Our results show that N_O and C_O act as deep acceptors, F_O, Cl_O, and S_P act as shallow donors. NO and CO have high formation energies under O-poor condition therefore they are not suitable for *p*-type doping Ag_3PO_4. Though F_O, Cl_O, and S_P have shallow transition energies, they have high formation energies, thus F_O, Cl_O, and S_P may be compensated by the intrinsic defects (such as Ag vacancy) and they are not possible lead to *n*-type conductivity in Ag_3PO_4.

Since Honda and Fujishima first discovered the photocatalytic water splitting into H_2 and O_2[1], the photocatalysis of water splitting has become an active research field and a potential way to solve the severe environmental crisis and energy shortage issues[2,3]. TiO_2 is the earliest photocatalyst used in water splitting, the intrinsic wide band gap of pure TiO_2 (~3.2 eV for anatase and ~3.0 eV for rutile) confines its photon absorption to the ultraviolet (UV) region, severely limiting solar energy utilization to ~5%[4]. Metal oxides are considered as potential candidates for photoelectrochemical (PEC) water splitting because of their resistance to oxidization and possible stability in aqueous solutions[5].

Recently, Ye *et al.* reported that cubic structure semiconductor Ag_3PO_4, which exhibits strong oxidation power leading to O_2 production from water, and its quantum yield achieve up to nearly 90% under visible light[6]. This is intriguing because most photocatalysts give much poorer quantum yields of ~20%[7]. Theoretical studies have also been performed to understand their origin[7–11]. Reunchan and Umezawa suggest that native point defects are unlikely to be responsible for an intrinsic conductivity of Ag_3PO_4, which an *n*-type character was observed in the previous report, but Ag_3PO_4 could feasibly be doped in *n*-type fashion[7].

First-principles density functional theory (DFT) calculations have been commonly used to study the electronic properties of point defects insulators and semiconductors. The local density approximation (LDA)[12] or the generalized gradient approximation (GGA)[13] functional are typically employed to describe the exchange-correlation energy within DFT. A major shortcoming of LDA and GGA calculations is the large uncertainty in the position of defect levels (and hence also formation energies) due to the severe underestimation of the semiconductor band gap. Heyd *et al.* recently proposed hybrid Hartree-Fock (HF) density functional[14], the hybrid functional has been used to accurately reproduce the band gap of insulators and semiconductors, therefore, the use of the hybrid functional is rationalized for the description of defect physics[15–18].

In this paper, we perform first-principles calculations based on the hybrid HF density functional to investigate the influence of N, C, F, Cl, and S impurities on the electronic properties of Ag_3PO_4. Because

[1]Department of Physics, Yunnan University, Kunming 650091, China. [2]Department of Physics, Hangzhou Normal University, Hangzhou 310036, China. Correspondence and requests for materials should be addressed to Y.H. (email: yhe@ynu.edu.cn)

interstitials of these impurities usually have large formation energies, we will only consider substitutional defects. The paper is organized as follow: Details of the calculations are provided in Sec. II. The electronic properties of each impurity are described in Sec. III. Finally, Sec. IV summarizes the results.

Methodology

The density functional calculations were performed in the Vienna *ab initio* simulation package (VASP)[19,20]. Interaction between the valence and core electrons was described using the projector augmented wave (PAW) approach[21]. A plane-wave basis set was used to expand the wave functions up to a kinetic energy cutoff value of 300 eV.

We used the Heyd-Scuseria-Ernzerhof hybrid functional (HSE06)[14,22], which adopts a screened Coulomb potential. Hence, greatly improving the description of structural properties and band structures, including band gaps. Both of these aspects are particularly important for defects. The HSE exchange is derived from the PBE0 (Perdew-Burke-Ernzerhof (PBE) functional containing 25% exact exchange)[23] exchange by range separation and then by elimination of counteracting long-range contributions as[4].

$$E_x^{HSE} = aE_x^{HF,SR}(\omega) + (1 - a)E_x^{PBE,SR}(\omega) + E_x^{PBE,SR}(\omega)$$

Where a is the mixing coefficient and ω is the range-separation parameter. A consistent screening parameter of $\omega = 0.2$ Å^{-1} is used for the semilocal PBE exchange as well as for the screened nonlocal exchange as suggested for the HSE06 functional[24]. We find that a proportion of 33% HF exchange with 67% PBE exchange produces accurate values for lattice constants and the band gap in Ag_3PO_4.

We used a 128-atom supercell constructed by $2 \times 2 \times 2$ replication of the cubic Ag_3PO_4 unit cell (space group $P\bar{4}3n$), which ensures sufficient spatial separation between the periodic images of the impurities. Various dopings of Ag_3PO_4 have been modeled by substitution of S at P or Y (Y = N, C, F, Cl) at O sites. For geometry optimizations and electronic structure calculations, the Brillouin zone was sampled with a $2 \times 2 \times 2$ mesh of Monkhorst-Pack special k-points[25]. Both the atomic positions and cell parameters were optimized until residual forces were below 0.01 eV/Å.

Formation energies and transition levels. To determine the defect formation energies and defect transition energy levels, we follow the procedure in Ref. 26. The defect formation energy $\Delta H_f(\alpha, q)$ as a function of the electron Fermi energy[27] E_F as well as the atomic chemical potentials[28,29] μ_i is as follows:

$$\Delta H_f(\alpha, q) = \Delta E(\alpha, q) + \sum n_i \mu_i + qE_F \quad (1)$$

Where

$$\Delta E(\alpha, q) = E(\alpha, q) - E(\text{host}) + \sum n_i E(i) + q\varepsilon_{\text{VBM}}(\text{host})$$

$E(\alpha, q)$ is the total energy for the studied supercell containing defect α in charge state q and E (host) is the total energy of the same supercell without the defect. n_i indicates the number of atoms of type i (host atoms or impurity atoms) that have been added to ($n_i < 0$) or removed from ($n_i > 0$) the supercell , and q is the number of electrons transferred from the supercell to the reservoirs in forming the defect cell. E_F is the electron Fermi level referenced to the valence-band maximum (VBM) of host, ε_{VBM}(host), and varies from the valence-band maximum to the conduction-band minimum (CBM). μ_i is the chemical potential of constituent i referenced to its elemental solid or gas with energy $E(i)$.

The defect transition energy level $\varepsilon_\alpha(q/q')$ is the E_F in Eq. (1), at which the formation energy $\Delta H_f(\alpha, q)$ of defect α in charge state q is equal to that of another charge q' of the same defect, i.e.,

$$\varepsilon_\alpha(q/q') = [\Delta E(\alpha, q) - \Delta E(\alpha, q')/(q' - q) \quad (2)$$

In this paper, we used a hybrid scheme to combine the advantages of both special k-points and Γ-point-only approaches[12]. In this scheme, for acceptor level ($q < 0$), the transition energy level with respect to VBM is given by:

$$\varepsilon(0/q) = [\varepsilon_D^\Gamma(0) - \varepsilon_{\text{VBM}}^\Gamma(\text{host})] + \{E(\alpha, q) - [E(\alpha, 0) - q\varepsilon_D^k(0)]\}/(-q) \quad (3)$$

For donor level ($q > 0$), the ionization energy referenced to the CBM is given by:

$$\varepsilon_g^\Gamma(\text{host}) - \varepsilon(0/q) = \left[\varepsilon_{\text{CBM}}^\Gamma(\text{host}) - \varepsilon_D^\Gamma(0)\right] + \left\{E(\alpha, q) - \left[E(\alpha, 0) - q\varepsilon_D^k(0)\right]\right\}/q \quad (4)$$

Where $\varepsilon_D{}^k(0)$ and $\varepsilon_D{}^\Gamma(0)$ are the defect levels at the special k-points (averaged) and at the Γ-point, respectively; $\varepsilon_{\text{VBM}}{}^\Gamma$(host) and $\varepsilon_{\text{CBM}}{}^\Gamma$(host) are the VBM and CBM energies, respectively, of the host at the Γ-point; and $\varepsilon_g{}^\Gamma$(host) is the calculated bandgap at the Γ-point.The formation energy of a charged defect is then given by

$$\Delta H_f(\alpha, q) = \Delta H_f(\alpha, 0) - q\varepsilon(0/q) + qE_F \quad (5)$$

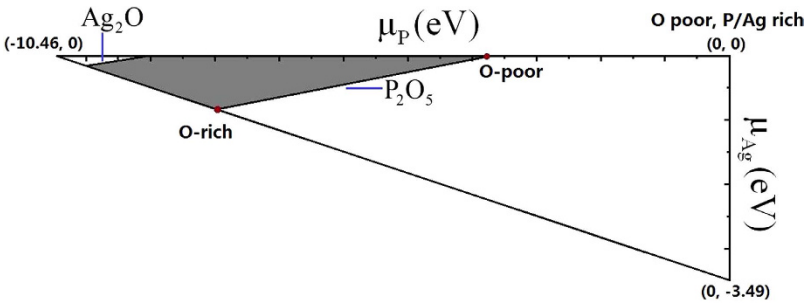

Figure 1. Accessible range of chemical potentials (shaded region) of equilibrium growth condition for Ag_3PO_4.

Where $\Delta H_f(\alpha, 0)$ is the formation energy of the charge-neutral defect. More details of calculation methods for formation energies and transition energies of defects are described elsewhere[30].

Chemical potentials. Under thermal equilibrium growth conditions, the steady production of host material, Ag_3PO_4, should satisfy the following equation:

$$3\mu_{Ag} + \mu_P + 4\mu_O = \Delta H_f(Ag_3PO_4) = -10.46eV \quad (6)$$

where μ_{Ag}, μ_P, and μ_O are the chemical potentials of Ag, P, and O source, respectively, and ΔH_f is the formation energy for Ag_3PO_4 per formula. In order to avoid the precipitation of the host elements, the chemical potential μ_i must be bound by

$$\mu_i < 0 \quad (7)$$

To avoid the formation of secondary phases (such as Ag_2O and P_2O_5), μ_{Ag}, μ_P, and μ_O must satisfy further constrains:

$$2\mu_{Ag} + \mu_O < \Delta H_f(Ag_2O) = -0.32eV \quad (8)$$

$$2\mu_P + 5\mu_O < \Delta H_f(P_2O_5) = -15.86eV \quad (9)$$

Considering Eqs. (6)–(9), the accessible ranges for μ_{Ag}, μ_P, and μ_O are limited and are presented as the shaded area in Fig. 1. As shown in Eqs. (5), the calculated formation energies of charged defects depend sensitively on the selected values for μ_{Ag}, μ_P, and μ_O and the Fermi-level positions. Here, the calculated values at two representative chemical potential points are labeled as O-rich and O-poor in Fig. 1. The exact value of chemical potentials at points O-rich condition and O-poor condition are $(-0.84, -7.93, 0)$ and $(0, -3.71, -1.69)$ for μ_{Ag}, μ_P, and μ_O, respectively.

For impurity doping, the chemical potentials of impurities also need to satisfy other constraints to avoid the formation of impurity-related phases, for example

$$\mu_{Ag} + \mu_{Cl} < \Delta H_f(AgCl) \quad (10)$$

$$\mu_S + 2\mu_{Ag} + 4\mu_O < \Delta H_f(Ag_2SO_4) \quad (11)$$

$$\mu_C + 2\mu_O < \Delta H_f(CO_2) \quad (12)$$

$$\mu_{Ag} + \mu_F < \Delta H_f(AgF) \quad (13)$$

The formation enthalpies of the AgCl, Ag_2SO_4, AgF, and CO_2 compounds obtained using the present HSE06 functional are listed in Table 1. The formation enthalpies obtained with the present HSE06 functional calculations are agreement with the experimental values.

Results and Discussion

Bulk properties. We first present the results for the structural and electronic properties of defect-free bulk Ag_3PO_4. The crystal structure of Ag_3PO_4 has a cubic structure with space group $P\bar{4}3n$, its basic structural unit is constructed by PO_4 tetrahedron and AgO_4 tetrahedron. The interaction between phosphorus and oxygen is mainly by covalent bond, while the interaction between silver and oxygen is formed

	HSE06	Experiment
ΔH_f (Ag_2O)	−0.32	−0.32[31]
ΔH_f (P_2O_5)	−15.86	−15.60[32]
ΔH_f (AgCl)	−1.20	−1.32[31]
ΔH_f (Ag_2SO_4)	−7.06	−7.42[31]
ΔH_f (AgF)	−2.03	−2.13[31]
ΔH_f (CO_2)	−3.82	−4.08[31]

Table 1. The formation enthalpies (in eV) of Ag_2O, P_2O_5, AgCl, Ag_2SO_4, AgF, and CO_2 molecules calculated from the HSE06 hybrid functional. The experimental values are also listed for comparison.

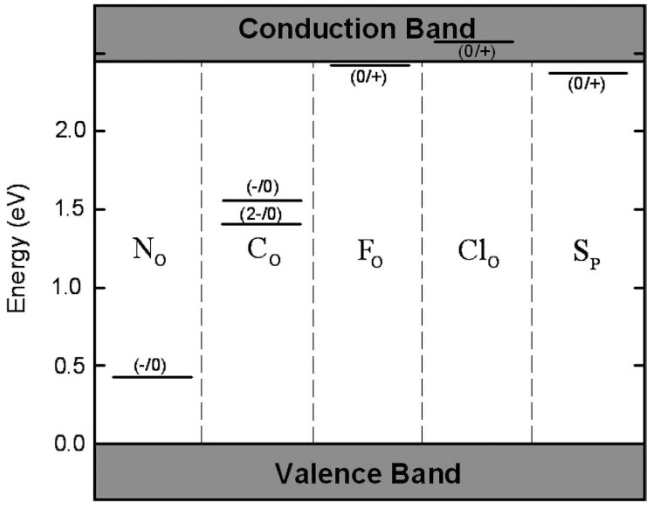

Figure 2. Thermodynamic transition levels for N, C, F, Cl and S impurities in Ag_3PO_4 (Unit: eV).

mainly by ionic bond[8]. The optimized cell parameters are $a = b = c = 6.02$ Å, and excellent agreement with the experimental values of $a = b = c = 6.00$ Å[8]. The P-O, Ag-O, and Ag-Ag bond lengths are calculated to be 1.56 Å (experimental value[11]: 1.56 Å), 2.37 Å (experimental value[11]: 2.36 Å), 3.01 Å (experimental value[11]: 3.00 Å), respectively. The calculated indirect band gap (M−Γ) is 2.33 eV, and the direct gap at Γ is 2.45 eV, in excellent agreement with the experimental value of 2.36 eV and 2.43 eV[6], respectively.

N, C, F, Cl, and S impurities in Ag_3PO_4. In this section, we discuss the different impurities in Ag_3PO_4 individually. The calculated thermodynamic transition energy levels for all impurities are listed in Fig. 2.

Nitrogen. The electronic properties of substitutional N at O sites (N_O) has been confirmed by several reports[4,5,33]. The conductivity of a semiconductor depends not only on the thermodynamic transition levels of donor and acceptors, but also on their formation energies. The thermodynamic transition level corresponds to the intersection of the formation energies for the different charge states. Formation energy as a function of Fermi level for N_O in the O-rich and O-poor limit are shown in Fig. 3. When the Fermi level is low, the neutral charge state (N_O^0) is energetically preferable, as the Fermi level rises, above the Fermi level of 0.46 eV, the negative charge state (N_O^{-1}) becomes more favorable. The thermodynamic transition level of $\varepsilon(-/0)$ is located at 0.46 eV above VBM. To obtain further details, the squared wave function $|\psi_e|^2$of the neutral defect state at Γ point is visualized in Fig. 4(a). The neutral defect state is highly confined around the N atom, which suggests that N_O^0 induces a localized defect state.

The N 2*p* orbital energy is 1.9 eV higher than the O 2*p* orbital energy, this imply that upon N substitution on O, the N 2*p* will create a partially filled impurity state at the Fermi level[35]. Thus, we examined the total density of states and projected density of states of N_O^0 (not shown). The neutral defect state has the main contribution from *s* orbitals and *d* orbitals of Ag, *p* orbitals of N and O, minor contribution from *p* orbitals of P. We also analyzed the local lattice relaxations around N_O^0 and N_O^{-1}. In the neutral state, the neighboring Ag atoms relax inward, resulting in a N-Ag bond length (2.11 Å) that is 11% shorter than the equilibrium O-Ag bond length, while the N-P bond length (1.65 Å) become 6% longer

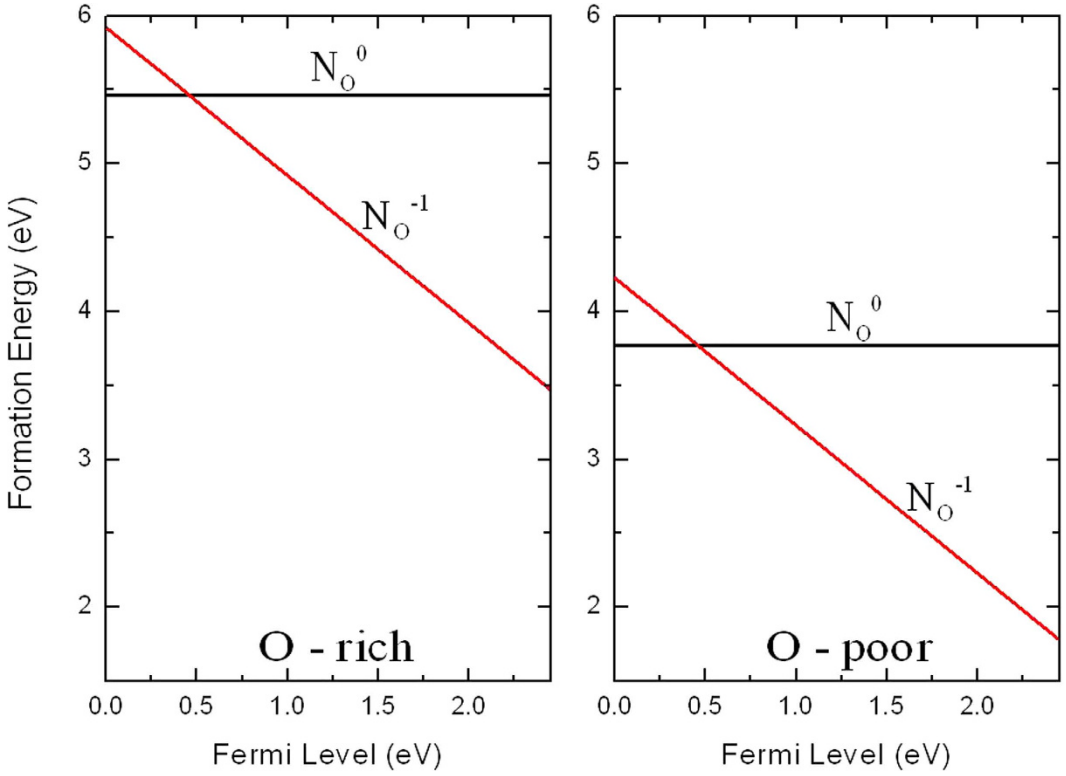

Figure 3. Calculated formation energies for N substituting on the O site as a function of Fermi level at O-rich and O-poor conditions.

than the equilibrium O-P bond length. In the negative state, the N-Ag bond length is 2.11 Å, while the N-P bond length 1.64 Å.

Figure 3 shows that the formation energy of N_O^0 is more stable than N_O^{-1} under O-poor condition but still relatively high even the Fermi level is near the conduction band. The high formation energy of the N_O indicates that the N-doped Ag_3PO_4 system using an N_2 source may not readily to produce *p*-type conductivity, which is consistent with the N-doped ZnO system[36].

Carbon. As carbon atom has four valence electrons which is two electrons less than oxygen atom, the substitution of C on O site (C_O) will act as a double acceptor. The 2*p* orbital energy of carbon is 3.8 eV higher than the O 2*p* orbital[35]. Consequently, C_O has two distinct transition levels in the band gap: a $\varepsilon(-/0)$ transition at 1.54 eV above the VBM and a $\varepsilon(2-/0)$ transition at 1.39 eV above the VBM as shown in Fig. 2. This implies that C_O in Ag_3PO_4 is a negative-*U* system. A defect often has a negative *U* if the atomic position of the defect depends sensitively on its charge state[37], *U* refers to the additional energy upon charging of the defect with an additional electron[38]. In the neutral charge state (C_O^0), the three Ag nearest neighbors relax inward by 13% (of the equilibrium O-Ag bond length) while one nearest P atom slightly relaxes outward by about 13% (of the equilibrium O-P bond length).

Figure 4(b) plots the squared wave function of the neutral C_O defect level. One can see that the squared wave function is localized around C atom, consistent with the deep level feature. The neutral defect state has *p* orbitals of C and O, *s* orbitals and *d* orbitals of Ag contribute primarily, *p* orbitals of P contribute in a small part. The formation energies of C_O in the neutral, −1, and −2 charge states as a function of the Fermi level are shown in Fig. 5. Even the formation energies of C_O under O-poor condition is significantly lower than under O-rich condition but still relatively high, therefore C is not suitable for *p*-type doping Ag_3PO_4.

Fluorine. Shifting the Fermi level towards the conduction band, or in other words *n*-type conditions, likely enhance the photocatalytic activities in Ag_3PO_4[7]. In contrast to the N_O and C_O, the substitutional F at O site (F_O) exhibits distinct characteristics. Unlike the N_O and C_O, where the defect states are highly localized at impurities, the defect state induced by F_O is spatially distributed away from F as the delocalized state [see Fig. 4(c)]. The defect state has main contribution from *s* and *d* orbitals of Ag followed by *s* orbitals of F, O, and P. For F_O^0 the three nearest neighbor Ag atoms relax outward by 17%, while for F_O^{+1} the relaxation are outward by 18% of the equilibrium Ag-O bond length.

The formation energy of F_O in different charge states as a function of the Fermi level is shown in Fig. 6. When the Fermi level is low, the positive charge state (F_O^{+1}) is energetically preferable, as the

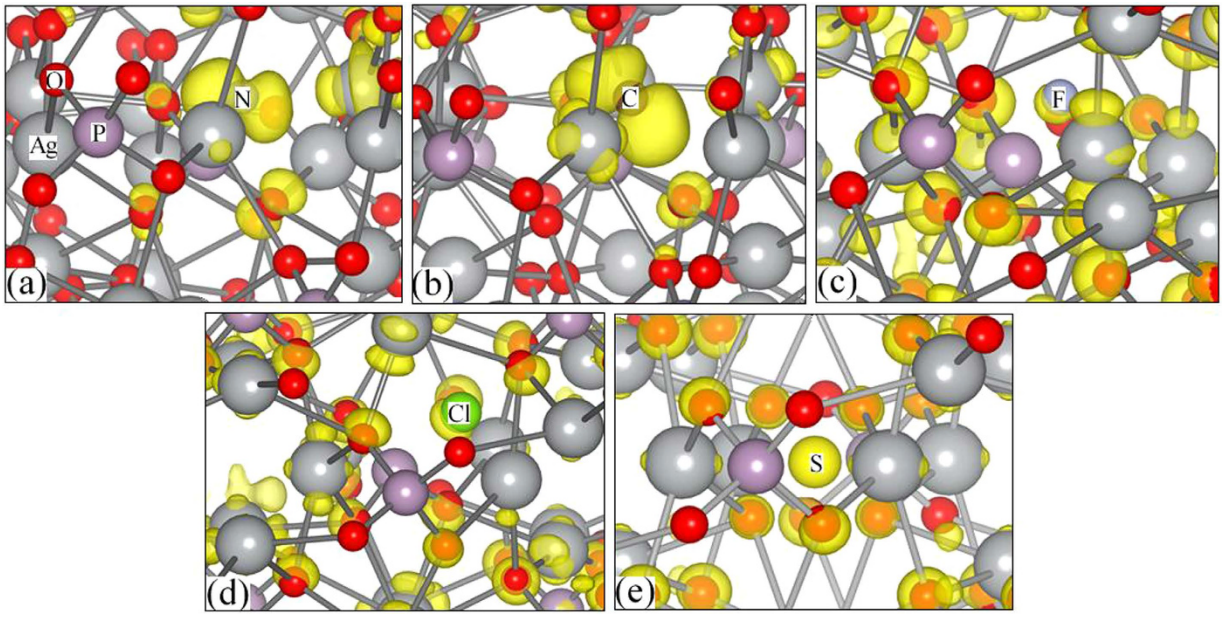

Figure 4. Spatial distribution of the squared wave functions $|\psi_e|^2$ of the neutral defect states created by (**a**) N_O, (**b**) C_O, (**c**) F_O, (**d**) Cl_O, (**e**) S_P, where the isosurface values[34] are 0.05, 0.05, 0.005, 0.005, 0.005 e/Å^3, respectively. The silver, pink, red balls represent Ag, P, O atoms, respectively.

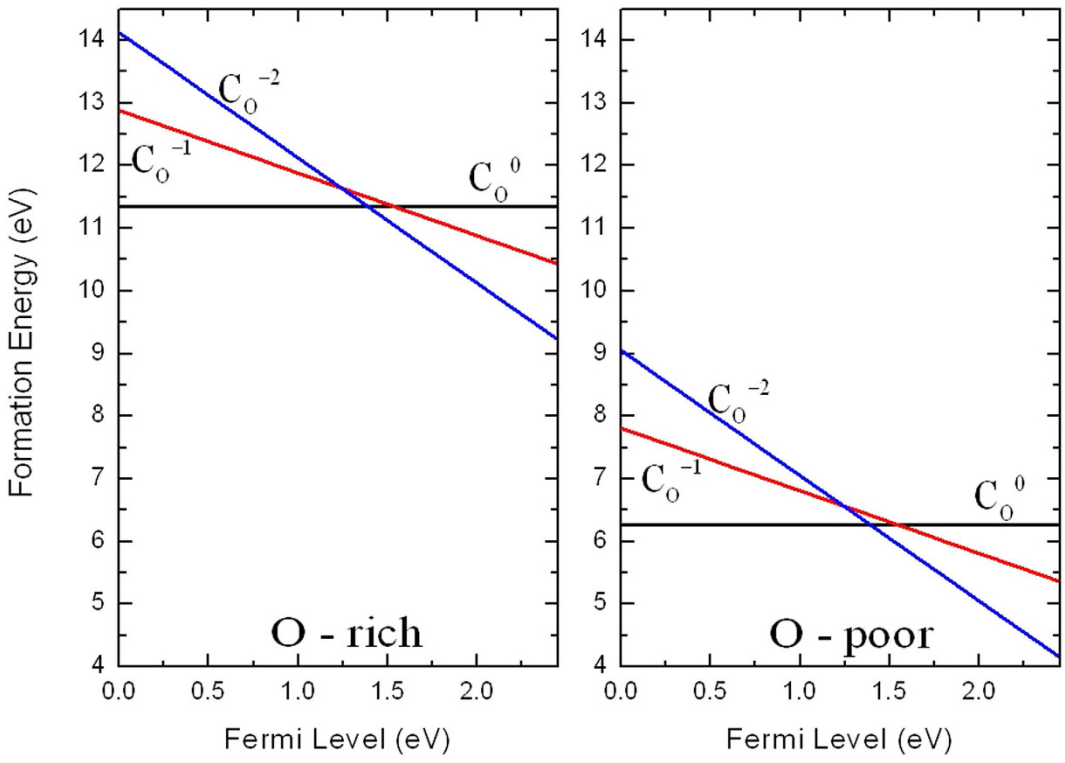

Figure 5. Calculated formation energies for C substituting on the O site as a function of Fermi level at O-rich and O-poor conditions.

Fermi level rises, the formation energy approaches that of the neutral charge state (F_O^0), above the Fermi level of 2.41 eV, the neutral charge state becomes more favorable. The thermodynamic transition level of $\varepsilon(0/+)$ is located 2.41 eV above the VBM (0.04 eV below the CBM). Though the Fermi level drops to the VBM the formation energy of F_O becomes very small for the favorable growth condition (O-poor

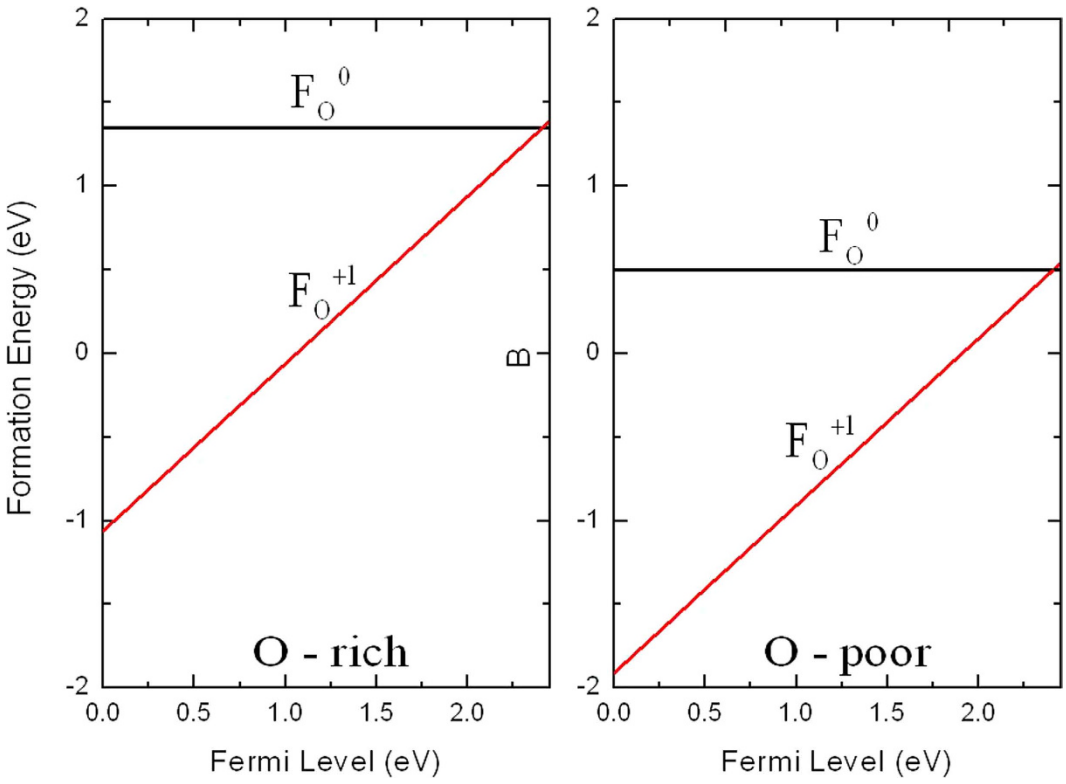

Figure 6. Calculated formation energies for F substituting on the O site as a function of Fermi level at O-rich and O-poor conditions.

condition), but when the Fermi level is near the CBM, the formation energy of F_O is still relatively high, thus, F_O may be compensated by Ag vacancy and it is not possible lead to *n*-type conductivity in Ag_3PO_4.

Chlorine. Chlorine atom is a famous *n*-type dopant[37,39]. The formation energy of substitutional Cl (Cl_O) against the Fermi level is shown in Fig. 7 for the two extreme cases. For Cl_O, no transition level is find in the gap (a $\varepsilon(0/+)$ transition at 0.14 eV above the CBM) and the +1 charge state is energetically favorable for the whole range of the Fermi level. The extra electron from Cl_O^0 occupies a conduction-band-like state, i.e., an extended state that is only slightly perturbed by the presence of the impurity[33]. Therefore, Cl_O is a shallow donor.

We have plotted the squared wave function of the neutral defect state at the Γ point in Fig. 4(d). It is seen that the squared wave function associated with the donor level distributed not only around Cl atom, but also around O atoms and Ag atoms away from the Cl atom, indicating a delocalized feature, which is consistent with the result that Cl_O is a shallow donor. The defect state has main contribution from *s* and *d* orbitals of Ag followed by *s* and *p* orbitals of Cl, O, and P. The formation energy of Cl_O is relatively high even under O-poor condition, therefore chlorine is not suitable for *n*-type doping Ag_3PO_4.

Sulfur. Sulfur is a possible candidate for *n*-type doping when substituted for P[7]. In the case of the S substituting on the P site, the transition level $\varepsilon(0/+)$ is located at 2.37 eV (0.08 eV below the CBM). The defect state is spatially away from S_P^0 [Fig. 4(e)], which is consistent with the result that S_P is a shallow donor. The defect state has main contribution from *s* and *d* orbitals of Ag followed by *s* orbitals of S, O, and P. It is also clearly from the shape of wave function that *s* and *d* orbitals are the main contributor to the defect state.

Sulfur is surrounded by four O atoms, for S_P^0 these four nearest neighbor O atoms relax inward by 4% of the equilibrium P-O bond length. Formation energies of S_P in its various charge state are shown in Fig. 8. We note, S_P has lower formation energy than F_O and Cl_O for both O-rich and O-poor conditions. When the Fermi level near the VBM, S_P is stable in the +1 charge state. In *n*-type Ag_3PO_4, where the Fermi level is near the CBM, S_P is stable in the neutral charge state, but the formation energies in the *n*-type regime are high under O-poor condition for this sulfur is not suitable candidate for *n*-type doping Ag_3PO_4.

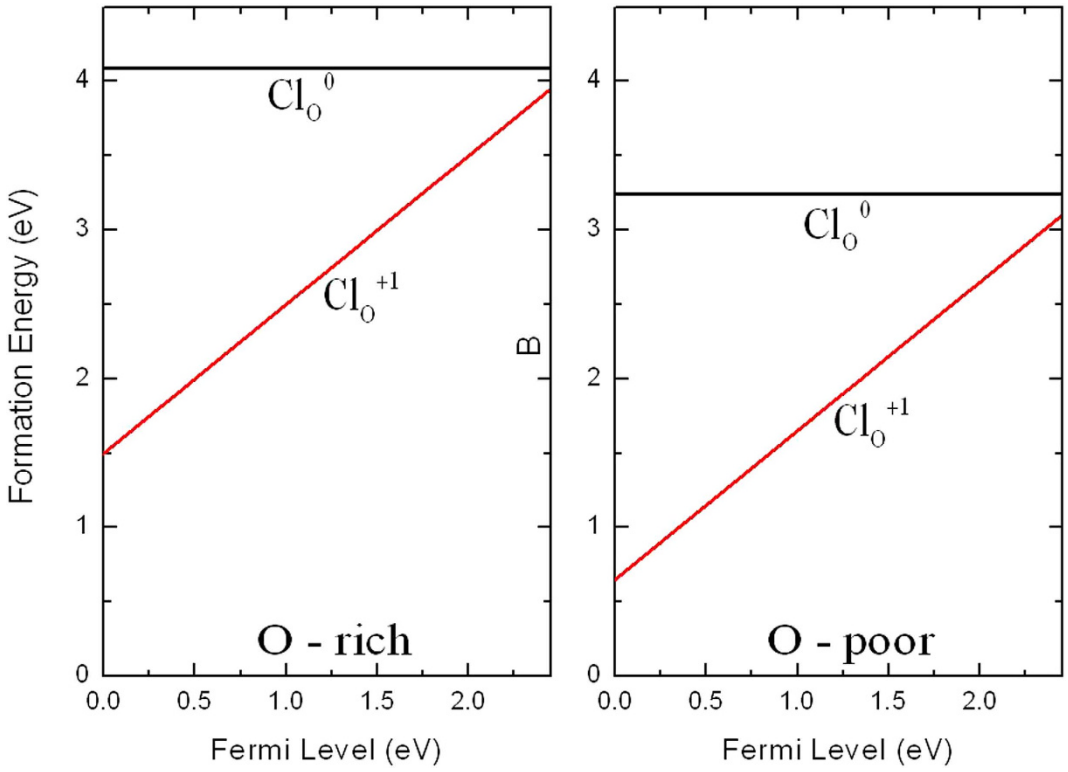

Figure 7. Calculated formation energies for Cl substituting on the O site as a function of Fermi level at O-rich and O-poor conditions.

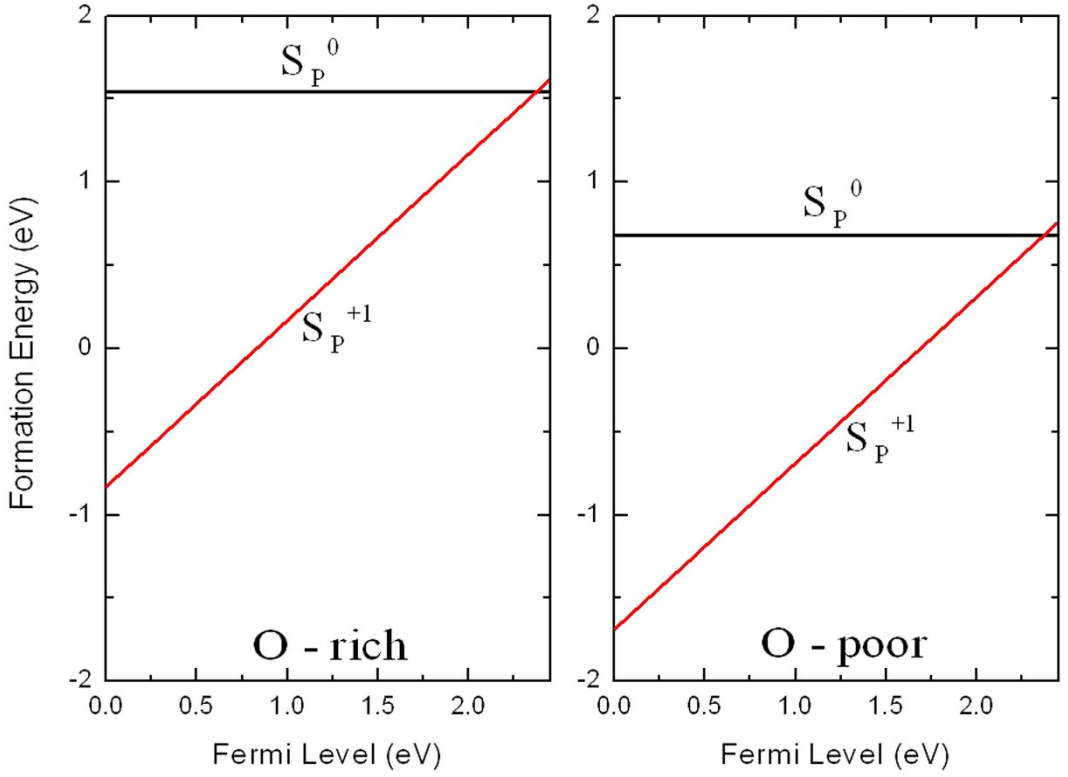

Figure 8. Calculated formation energies for S substituting on the P site as a function of Fermi level at O-rich and O-poor conditions.

Conclusion

Using hybrid density functional calculations we have investigated the electrical properties of N, C, F, Cl, and S impurities in Ag_3PO_4. We found that N_O and C_O act as deep acceptors, F_O, Cl_O, and S_P act as shallow donors. N_O and C_O have high formation energies even under most equilibrium condition (O-poor condition) therefore they are not suitable for *p*-type doping Ag_3PO_4. Though F_O, Cl_O, and S_P have shallow transition energies, they have high formation energies, thus F_O, Cl_O, and S_P may be compensated by Ag vacancy and they are not possible lead to *n*-type conductivity in Ag_3PO_4.

References

1. Fujishima, A. & Honda, K. Electrochemical Photolysis of Water at a Semiconductor Electrode. *Nature (London)* **238,** 37 (1972).
2. Lai, K., Zhu, Y., Dai, Y. & Huang, B. Intrinsic defect in $BiVO_4$: A density functional theory study. *J. Appl. Phys.* **112,** 043706 (2012).
3. Wang, D. F., Zou, Z. G. & Ye, J. H. Photocatalytic Water Splitting with the Cr-Doped $Ba_2In_2O_5/In_2O_3$ Composite Oxide Semiconductors. *Chem. Mater.* **17,** 3255 (2005).
4. Çelik, V. & Mete, E. Range-separated hybrid exchange-correlation functional analyses of anatase TiO_2 doped with W, N, S, W/N, or W/S. *Phys. Rev. B* **86,** 205112 (2012).
5. Yin, W. J. *et al.* Doping properties of monoclinic $BiVO_4$ studied by first-principles density-functional theory. *Phys. Rev. B* **83,** 155102 (2011).
6. Yi, Z. *et al.* An orthophosphate semiconductor with photooxidation properties under visible-light irradiation. *Nat. Mater.* **9,** 559 (2010).
7. Reunchan, P. & Umezawa, N. Native defects and hydrogen impurities in Ag_3PO_4. *Phys. Rev. B* **87,** 245205 (2013).
8. Liu, J. J. *et al.* Electronic structure and optical properties of Ag_3PO_4 photocatalyst calculated by hybrid density functional method. *Appl. Phys. Lett.* **99,** 191903 (2011).
9. Ma, X. *et al.* Origin of photocatalytic activation of silver orthophosphate from first-principles. *J. Phys. Chem. C* **115,** 4680 (2011).
10. Ma, Z., Yi, Z., Sun, J. & Wu, K. Electronic and Photocatalytic Properties of $Ag_3PC_4^{VI}$ (C = O, S, Se): A Systemic Hybrid DFT Study. *J. Phys. Chem. C* **116,** 25074 (2012).
11. Umezawa, N., Shuxin, O. & Ye, J. Theoretical study of high photocatalytic performance of Ag_3PO_4. *Phys. Rev. B* **83,** 035202 (2011).
12. Ceperley, D. M. & Alder, B. J. Ground State of the Electron Gas by a Stochastic Method. *Phys. Rev. Lett.* **45,** 566 (1980).
13. Perdew, J. P., Burke, K. & Ernzerhof, M. Generalized Gradient Approximation Made Simple. *Phys. Rev. Lett.* **77,** 3865 (1996).
14. Heyd, J., Scuseria, G. E. & Ernzerhof, M. Hybrid functionals based on a screened Coulomb potential. *J. Chem. Phys.* **124,** 219906 (2006).
15. Shimada, T., Ueda, T., Wang, J. & Kitamura, T. Hybrid Hartree-Fock density functional study of charged point defects in ferroelectric $PbTiO_3$. *Phys. Rev. B* **87,** 174111 (2013).
16. Lyons, J. L., Janotti, A. & Van de Walle, C. G. Effects of carbon on the electrical and optical properties of InN, GaN, and AlN. *Phys. Rev. B* **89,** 035204 (2014).
17. Chen, S., Narang, P., Atwater, H. A. & Wang, L.-W. Phase Stability and Defect Physics of a Ternary $ZnSnN_2$ Semiconductor: First Principles Insights. *Adv. Mater.* **26,** 311 (2014).
18. Choi, M., Janotti, A. & Van de Walle, C. G. Native point defects in $LaAlO_3$: A hybrid functional study. *Phys. Rev. B* **88,** 214117 (2013).
19. Kresse, G. & Furthmüller, J. Efficient iterative schemes for *ab initio* total-energy calculations using a plane-wave basis set. *Phys. Rev. B* **54,** 11169 (1996).
20. Kresse, G. & Joubert, D. From ultrasoft pseudopotentials to the projector augmented-wave method. *Phys. Rev. B* **59,** 1758 (1999).
21. Blöchl, P. E. Projector augmented-wave method. *Phys. Rev. B* **50,** 17953 (1994).
22. Kohn, W. & Sham, L. J. Self-Consistent Equations Including Exchange and Correlation Effects. *Phys. Rev.* **140,** A1133 (1965).
23. Perdew, J. P., Burke, K. & Ernzerhof, M. Generalized Gradient Approximation Made Simple. *Phys. Rev. Lett.* **77**, 3865 (1996); **78,** 1396 (1997).
24. Krukau, A. V., Vydrov, O. A., Izmaylov, A. F. & Scuseria, G. E. Influence of the exchange screening parameter on the performance of screened hybrid functionals. *J. Chem. Phys.* **125,** 224106 (2006)
25. Monkhorst, H. J. & Pack, J. D. Special points for Brillouin-zone integrations. *Phys. Rev. B* **13,** 5188 (1976).
26. Wei, S.-H. Comput. Overcoming the doping bottleneck in semiconductors. *Comput. Mater. Sci.* **30,** 337 (2004).
27. Baraff, G. A. & Schluter, M. Electronic Structure, Total Energies, and Abundances of the Elementary Point Defects in GaAs. *Phys. Rev. Lett.* **55,** 1327 (1985).
28. Zhang, S. B. & Northrup, J. E. Chemical potential dependence of defect formation energies in GaAs: Application to Ga self-diffusion. *Phys. Rev. Lett.* **67,** 2339 (1991).
29. Laks, D. B. *et al.* Native defects and self-compensation in ZnSe. *Phys. Rev. B* **45,** 10965 (1992).
30. Yan, Y. & Wei, S.-H. Phys. Doping asymmetry in wide-bandgap semiconductors: Origins and solutions. *Phys. Stat. Sol. (b)* **245,** 641 (2008).
31. David R. Lide, ed., *CRC Handbook of Chemistry and Physics, 90th Edition (Internet Version 2010)*, CRC Press/Taylor and Francis, Boca Raton, FL. (2010)
32. Jung, In-Ho & Hudon, P. Thermodynamic Assessment of P_2O_5. *J. Am. Ceram. Soc.*, **95,** 3665 (2012)
33. Varley, J. B., Janotti, A. & Van de Walle, C. G. Group-V impurities in SnO_2 from first-principles calculations. *Phys. Rev. B* **81,** 245216 (2010).
34. Momma, K. & Izumi, F. *VESTA*: a three-dimensional visualization system for electronic and structural analysis. *J. Appl. Crystallogr.*, **41,** 653 (2008).
35. Wang, B. C. *et al.* Band gap engineering in $BiNbO_4$ for visible-light photocatalysis. *Appl. Phys. Lett.* **100,** 182102 (2012).
36. Duan, X. M., Stampfl, C., Bilek, M. M. M. & Mackenzie, D. R. Codoping of aluminum and gallium with nitrogen in ZnO: A comparative first-principles investigation. *Phys. Rev. B* **79,** 235208 (2009).
37. Wei, Su-Huai & Zhang, S. B. Chemical trends of defect formation and doping limit in II-VI semiconductors: The case of CdTe. *Phys. Rev. B* **66,** 155211 (2002).
38. Grundmann, M. *The Physics of Semiconductors*, 2nd ed. (Springer, Berlin, 2010).
39. Varley, J. B., Weber, J. R., Janotti, A. & Van de Walle, C. G. Oxygen vacancies and donor impurities in β-Ga_2O_3. *Appl. Phys. Lett.* **97,** 142106 (2010).

Acknowledgments

We sincerely thank Dr. Jyh-Pin Chou for his valuable discussions. This work was supported by National Natural Science Foundation of China (Grant No. 61366007 and No. 11164032 and No. 61066005), Program for New Century Excellent Talents in University (Grant No. NCET-12-1080), Applied Basic Research Foundation of Yunnan Province (Grant No. 2011CI003 and No. 2013FB007), Program for Excellent Young Talents in Yunnan University. Computational resources were provided by the High Performance Computing Center of Yunnan University.

Author Contributions

Yang Huang carried out the DFT calculations and prepared the manuscript. T.M., Q.C., C.C. and Y.H. Contributed the discussion and suggestions. All authors read the manuscript.

Additional Information

Competing financial interests: The authors declare no competing financial interests.

How to cite this article: Huang, Y. *et al.* The electronic properties of impurities (N, C, F, Cl, and S) in Ag_3PO_4: A hybrid functional method study. *Sci. Rep.* **5**, 12750; doi: 10.1038/srep12750 (2015).